Unpolarized Structure Functions at Jefferson Lab

M. E. Christy[1] **and W. Melnitchouk**[2]

[1] Hampton University, Hampton, Virginia 23668, USA
[2] Jefferson Lab, Newport News, Virginia 23606, USA

Abstract. Over the past decade measurements of unpolarized structure functions with unprecedented precision have significantly advanced our knowledge of nucleon structure. These have for the first time allowed quantitative tests of the phenomenon of quark-hadron duality, and provided a deeper understanding of the transition from hadron to quark degrees of freedom in inclusive scattering. Dedicated Rosenbluth-separation experiments have yielded high-precision transverse and longitudinal structure functions in regions previously unexplored, and new techniques have enabled the first glimpses of the structure of the free neutron, without contamination from nuclear effects.

1. Introduction

Throughout the modern history of nuclear and particle physics, measurements of structure functions in high-energy lepton-nucleon scattering have played a pivotal role. The demonstration of structure function scaling in early deep-inelastic scattering (DIS) experiments at SLAC in the late 1960's [1] established the reality of quarks as elementary constituents of protons and neutrons — a feat recognized by the award of the 1990 Nobel Prize in Physics to Friedman, Kendall and Taylor. This paved the way to the development of quantum chromodynamics (QCD) as the theory of strong nuclear interactions, and its subsequent confirmation several years later through the discovery of logarithmic scaling violations in structure functions [2].

The interpretation of structure functions in terms of quark and gluon (or parton) momentum distributions resulted in the emergence of a remarkably simple and intuitive picture of the nucleon [3], allowing a vast amount of scattering data to be described in terms of a few universal functions — the parton distribution functions (PDFs). At leading order (LO) in α_s, the F_2 structure function of the proton, for example, could be simply represented as a charge squared-weighted sum of PDFs,

$$F_2 = \sum_q e_q^2 \, x(q + \bar{q}) = \frac{4}{9}x(u + \bar{u}) + \frac{1}{9}x(d + \bar{d}) + \frac{1}{9}x(s + \bar{s}) + \cdots, \qquad (1)$$

where q and $\bar{q}$ are the quark and antiquark momentum distribution functions, usually expressed as functions of the momentum fraction x of the nucleon carried by the parton, at a scale given by the momentum transfer squared Q^2.

Over the ensuing decades concerted experimental DIS programs at SLAC, CERN, DESY and Fermilab have provided a detailed mapping of the PDFs over a large range of kinematics, with Q^2 and x spanning several orders of magnitude. To manage the ever increasing number of data sets, from not only inclusive DIS but also other high energy processes such as Drell-Yan, W-boson and jet production in hadronic collisions at Fermilab, sophisticated global fitting

efforts were developed [4, 5, 6, 7] that now include perturbative corrections calculated to next-to-leading order (or higher) in the strong coupling constant α_s. With the increasing energies available at facilities such as the DESY ep collider HERA (and in future the Large Hadron Collider at CERN), PDF studies turned their attention primarily to exploring the region of very small x (down to $x \sim 10^{-6}$), where the structure of the nucleon is dominated by its sea quark and gluon distributions. However, while opening the door to exploration of phenomena such as saturation and Q^2 evolution in new kinematic regimes, one can argue whether DIS at low x measures the intrinsic structure of the nucleon or the hadronic structure of the virtual photon, γ^*. Because the virtual photon in the DIS process can fluctuate into $q\bar{q}$ pairs whose coherence length $\lambda \sim 1/Mx$ becomes large at small x, DIS at $x \lesssim 0.1$ really probes the γ^*N interaction rather than the structure of the nucleon or the γ^* separately. At high x, in contrast, the virtual photon is point-like and unambiguously probes the structure of the nucleon [8].

Moreover, despite the impressive achievements over the past 4 decades, there are still some regions of kinematics where our knowledge of structure functions and PDFs remains unacceptably poor, with little progress made since the 1970's. A striking example is the region of large x ($x \gtrsim 0.5$), where most of the momentum is carried by valence quarks, and sea quarks and gluons are suppressed. Here the valence quark PDFs can be more directly related to quark models of hadron structure; however, the rapidly falling cross sections have made precision measurements extremely challenging. Another example is the pre-asymptotic region dominated by nucleon resonances, where data on the individual transverse and longitudinal cross sections at intermediate and high values of Q^2 are either nonexistent or have large uncertainties. With the availability of continuous, high luminosity electron beams at the CEBAF accelerator, the first decade of experiments at Jefferson Lab has seen a wealth of high-quality data on unpolarized structure functions of the nucleon, penetrating into the relatively unexplored large-x domain and the transition region between resonances and scaling.

The new data in the resonance region confirmed in spectacular fashion the phenomenon of quark-hadron duality in the proton F_2 structure function, and revealed intriguing details about the workings of duality in a number of other observables. The impact of this has been a re-evaluation of the applicability of perturbative QCD to structure functions at low Q^2, and has allowed a much larger body of data to be used in global PDF analyses [9]. Jefferson Lab has also set a new standard in the determination of Rosenbluth-separated longitudinal and transverse structure functions, which eliminates the need for model-dependent assumptions that have plagued previous extractions of structure functions from cross section data.

On the theoretical front, the region of large x and low Q^2 brings to the fore a number of issues which complicate structure function analysis, such as $1/Q^2$ suppressed target mass and higher twist corrections, and nuclear corrections when scattering from nuclear targets. Controlling these corrections requires more sophisticated theoretical tools to be developed, and has motivated theoretical studies, many of which are still ongoing. It has also paved the way towards the 12 GeV experimental program, in which structure functions will be measured to very high x in the DIS region, addressing some long-standing questions about the behavior of PDFs as $x \to 1$.

In the next section we summarize the kinematics and formalism relevant for inclusive lepton–nucleon scattering, including the key results from the operator product expansion. Measurements of the proton F_2^p structure functions and their moments are reviewed in Sec. 3, together with their role in the verification of quark-hadron duality. Data on the deuteron F_2^d structure function are presented in Sec. 4, and the extraction from these of the neutron F_2^n structure function F_2^n is discussed in Sec. 5. Section 6 reviews new measurements of the longitudinal structure function F_L, while Sec. 7 surveys results from semi-inclusive pion production. Finally, in Sec. 8 we describe the impact that the Jefferson Lab data have had on our understanding of nucleon structure in a global context, and briefly outline prospects for future measurements in the 12 GeV era.

2. Formalism

2.1. Kinematics

Because of the small value of the electromagnetic fine structure constant, $\alpha = e^2/4\pi$, the inclusive scattering of an electron from a nucleon, $e(k) + N(p) \rightarrow e'(k') + X$, can usually be approximated by the exchange of a single virtual photon, $\gamma^*(q)$, where $q = k' - k$. In terms of the laboratory frame incident electron energy E, the scattered electron energy E', and the scattering angle θ, the photon virtuality is given by $-q^2 \equiv Q^2 = 4EE' \sin^2 \theta/2$, where the electron mass has been neglected. The invariant mass squared of the final hadronic state X is $W^2 = (p+q)^2 = M^2 + 2M\nu - Q^2 = M^2 + Q^2(1-x)/x$, where M is the nucleon mass, $\nu = E - E'$ is the energy transfer, and $x = Q^2/2M\nu$ is the Bjorken scaling variable.

In the one photon exchange approximation the spin-averaged cross section for inclusive electron-nucleon scattering in the laboratory frame can be written as

$$\frac{d^2\sigma}{d\Omega dE'} = \frac{\alpha^2}{Q^4}\frac{E'}{E} L_{\mu\nu} W^{\mu\nu}, \tag{2}$$

where the leptonic tensor $L_{\mu\nu} = 2\left(k_\mu k'_\nu + k'_\mu k_\nu - g_{\mu\nu} k \cdot k'\right)$, and using constraints from Lorentz, gauge and parity invariance the hadronic tensor $W^{\mu\nu}$ can in general be written as

$$MW^{\mu\nu} = \left(-g^{\mu\nu} + \frac{q^\mu q^\nu}{q^2}\right) F_1(x, Q^2) + \left(p^\mu - \frac{p \cdot q}{q^2} q^\mu\right)\left(p^\nu - \frac{p \cdot q}{q^2} q^\nu\right)\frac{F_2(x, Q^2)}{p \cdot q}. \tag{3}$$

The structure functions F_1 and F_2 are generally functions of two variables, but become independent of the scale Q^2 in the Bjorken limit, in which both Q^2 and $\nu \rightarrow \infty$ with x fixed. At finite values of Q^2 a modified scaling variable is more appropriate [10, 11],

$$\xi = \frac{2x}{1+\rho}, \quad \text{with } \rho = \frac{|\boldsymbol{q}|}{\nu} = \sqrt{1 + Q^2/\nu^2}, \tag{4}$$

which tends to x in the Bjorken limit.

In terms of cross sections for absorbing helicity ± 1 (transverse) and helicity 0 (longitudinal) photons, σ_T and σ_L, the cross section can be written as

$$\frac{d^2\sigma}{d\Omega dE'} = \Gamma\left(\sigma_T(x, Q^2) + \epsilon\,\sigma_L(x, Q^2)\right), \tag{5}$$

where $\Gamma = (\alpha/2\pi^2 Q^2)(E'/E)K/(1-\epsilon)$ is the flux of transverse virtual photons, with the factor $K = \nu(1-x)$ in the Hand convention [12], and

$$\epsilon = \left[1 + 2\left(1 + \frac{\nu^2}{Q^2}\right)\tan^2\frac{\theta}{2}\right]^{-1} \tag{6}$$

is the relative flux of longitudinal virtual photons. Equating Eqs. (2) and (5), the structure functions can be written in terms of the photoabsorption cross sections as

$$F_1(x, Q^2) = \frac{K}{4\pi^2\alpha} M\sigma_T(x, Q^2), \tag{7}$$

$$F_2(x, Q^2) = \frac{K}{4\pi^2\alpha}\frac{\nu}{(1 + \nu^2/Q^2)}\left[\sigma_T(x, Q^2) + \sigma_L(x, Q^2)\right], \tag{8}$$

which reveals that F_1 is related only to the transverse virtual photon coupling, while F_2 is a combination of both transverse and longitudinal couplings. One can also define a purely longitudinal structure function F_L,

$$F_L = \rho^2 F_2 - 2xF_1 = 2xF_1 R, \tag{9}$$

where $R = \sigma_L/\sigma_T$ is the ratio of longitudinal to transverse cross sections.

The separation of the unpolarized structure functions into longitudinal and transverse parts from cross section measurements can be accomplished via the Rosenbluth, or longitudinal-transverse (LT), separation technique [13], by making measurements at two or more values of ϵ for fixed x and Q^2. Fitting the reduced cross section σ/Γ linearly in ϵ yields σ_T (and therefore F_1) as the intercept, while the ratio R is obtained from the slope. Note that F_2 can only be extracted from cross sections either by measuring at $\epsilon = 1$ or by performing LT separations. At typical Jefferson Lab kinematics the contribution of F_L to F_2 can be significant.

The above discussion assumed the dominance of the one-photon exchange amplitude in describing the neutron current electron scattering cross section. In principle there are additional contributions arising from the exchange of a Z boson, and in particular the interference between γ^* and Z exchange. The interference is in fact very relevant for parity-violating electron scattering, discussed elsewhere in this volume in connection with extractions of strange electromagnetic form factors from parity-violating asymmetries.

2.2. Operator product expansion

The theoretical basis for describing the Q^2 dependence of structure functions in QCD is Wilson's operator product expansion (OPE) [14]. The quantities most directly amenable to a QCD analysis are the *moments* of structure functions, the n-th moments of which are defined as

$$M_1^{(n)}(Q^2) \;=\; \int_0^1 dx \; x^{n-1} F_1(x, Q^2), \qquad M_{2,L}^{(n)}(Q^2) \;=\; \int_0^1 dx \; x^{n-2} F_{2,L}(x, Q^2). \qquad (10)$$

As will become relevant in the discussion of duality in Sec. 3 below, at large $Q^2 \gg \Lambda_{\mathrm{QCD}}^2$ the moments can be expanded in powers of $1/Q^2$, with the coefficients in the expansion given by matrix elements of local operators corresponding to a certain *twist*, τ, defined as the mass dimension minus the spin, n, of the operator. For the n-th moment of F_2, for instance, one has the expansion

$$M_2^{(n)}(Q^2) \;=\; \sum_{\tau=2,4\ldots}^{\infty} \frac{A_\tau^{(n)}(\alpha_s(Q^2))}{Q^{\tau-2}}, \qquad n = 2, 4, 6 \ldots \qquad (11)$$

where $A_\tau^{(n)}$ are the matrix elements with twist $\leq \tau$. As the argument suggests, the Q^2 dependence of the matrix elements can be calculated perturbatively, with $A_\tau^{(n)}$ expressed as a power series in $\alpha_s(Q^2)$. For twist two, the coefficients $A_2^{(n)}$ are given in terms of matrix elements of spin-n operators, $A_2^{(n)} p^{\mu_1} \cdots p^{\mu_n} + \cdots = \langle p | \bar{\psi} \gamma^{\{\mu_1} i D^{\mu_2} \cdots i D^{\mu_n\}} \psi | p \rangle$, where ψ is the quark field, D^μ is the covariant derivative, and the braces $\{\cdots\}$ denote symmetrization of indices and subtraction of traces.

The leading-twist terms correspond to diagrams such as in Fig. 1 (a), in which the virtual photon scatters incoherently from a single parton. The higher-twist terms in Eq. (11) are proportional to higher powers of $1/Q^2$ whose coefficients are matrix elements of local operators involving multi-quark or quark-gluon fields, such as those depicted in Fig. 1 (b) and (c). The higher twists therefore parametrize long-distance multi-parton correlations, which can provide clues to the dynamics of quark confinement.

The additional terms (referred to as the "trace terms") in the twist-two matrix elements involve structures such as $p^2 g^{\mu_i \mu_j}$ and are thus suppressed by powers of $p^2/Q^2 \sim Q^2/\nu^2$. While negligible in the Bjorken limit, at finite Q^2 these give rise to the so-called *target mass corrections* (TMCs), and are important in the analysis of Jefferson Lab data at large values of x. Because their origin is in the same twist-two operators that give rise to structure function scaling, TMCs
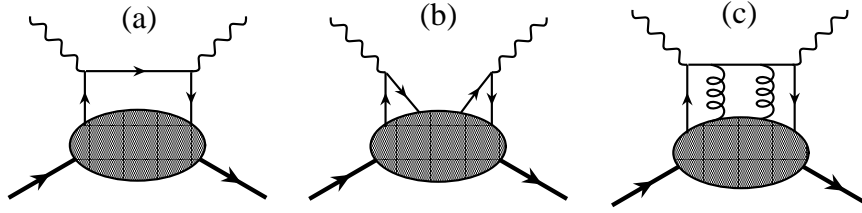
Figure 1. **(a)** Leading-twist ("handbag") contribution to the structure function, **(b)** higher-twist ("cat's ears") four-quark contributions, **(c)** higher-twist quark-gluon interactions.

are formally twist-two effects and are kinematical in origin. Inverting the expressions for the full moments including the trace terms, the resulting target mass corrected F_2 structure function in the OPE is given by [15, 16]

$$F_2^{\text{TMC}}(x, Q^2) = \frac{x^2}{\xi^2 \rho^3} F_2^{(0)}(\xi, Q^2) + \frac{6M^2 x^3}{Q^2 \rho^4} \int_\xi^1 du \left(1 + \frac{2M^2 x}{Q^2 \rho}(u - \xi)\right) \frac{F_2^{(0)}(u, Q^2)}{u^2}, \quad (12)$$

where $F_2^{(0)}$ is the structure function in the $M^2/Q^2 \to 0$ limit. Similar expressions are found for the F_1 and F_L structure functions [15, 16]. One should note, however, that the OPE result for TMCs to structure functions is not unique; in the collinear factorization approach, for example, in which parton distributions are formulated *a priori* in momentum space, different expressions for TMCs arise [17]. While both formalisms give the same results in the Bjorken limit, the differences between these at finite Q^2 can be seen as representing an inherent prescription dependence and systematic uncertainty in the analysis of structure functions at low Q^2.

3. Proton F_2 structure function

Measurements of the proton F_2^p structure function have been taken at Jefferson Lab over a range of kinematics, from Q^2 as low as 0.1 GeV^2 and below (to study the transition to the photoproduction point, $Q^2 = 0$) and up to $Q^2 = 8$ GeV^2 (to study the large-x behavior and quark-hadron duality). At the larger Q^2 values the high luminosity provided by the CEBAF accelerator has allowed significant improvement in the statistical precision of high-x measurements over all previous experiments. In addition, with the HMS spectrometer in Hall C well understood, LT separated cross sections have been measured with better than 1.6% systematic point-to-point uncertainties and typically less than 1.8% normalization uncertainties.

Precision F_2^p spectra extracted from cross sections measured in Hall C [18, 19, 20] are shown in Fig. 2 (left) as a function of x for several Q^2 values ($Q^2 = 0.5, 1.5, 3$ and 5.5 GeV^2), together with previous SLAC [21] and NMC [22] data at lower x. The data have been bin-centered to the common Q^2 values shown for all measurements within the range of 20% of the central value, utilizing a fit [23] to the DIS data and a global fit [24] to Jefferson Lab resonance region data. In addition to the Hall C measurements, there now also exists a large body of F_2^p data from Hall B covering a significant range of kinematics, which is afforded by the large acceptance of the CLAS spectrometer. An example of the F_2^p spectrum extracted from CLAS is shown in Fig. 2 (right) at $Q^2 = 0.775$ GeV^2. In Table 1 we present a complete list of all unpolarized inclusive and semi-inclusive measurements on the proton and deuteron performed at Jefferson Lab through 2010, including their current status.

3.1. Quark-hadron duality
The proton F_2^p data in Fig. 2 illustrate the intriguing phenomenon of quark-hadron duality, which relates structure functions in the nucleon resonance and DIS regions. First observed by
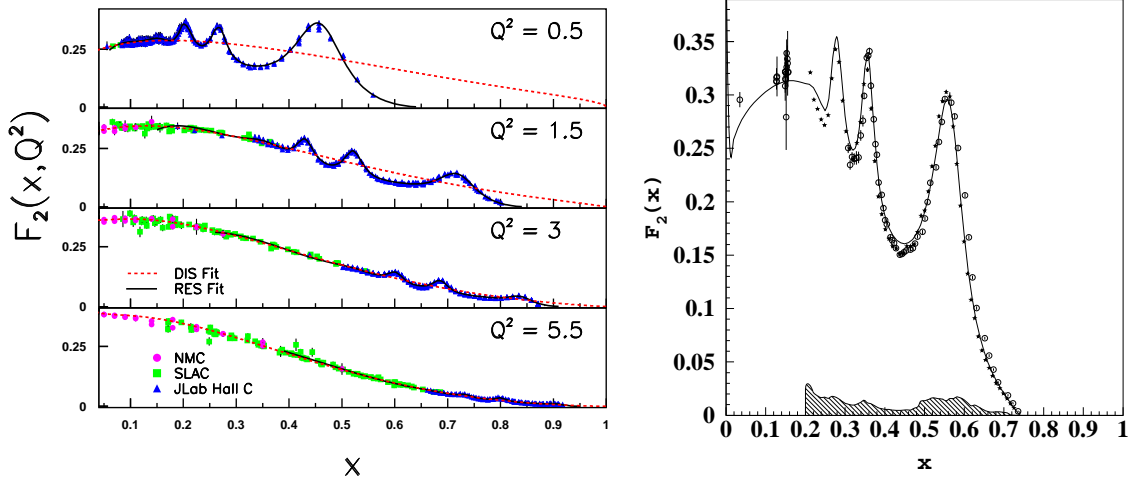
Figure 2. (*Left*) Proton F_2^p structure function data from Hall C [18, 19, 20], SLAC [21], and NMC [22] at $Q^2 = 0.5, 1.5, 3$ and 5.5 GeV^2, compared with a fit [24] to the transverse and longitudinal resonance cross sections from photoproduction to $Q^2 = 9$ GeV^2 (solid), and a global fit [23] to DIS data (dashed). (*Right*) Proton F_2^p from CLAS in Hall B at $Q^2 = 0.775$ GeV^2 (stars) [25], compared to earlier Hall C data (open circles) [26].

Bloom and Gilman [37] in the early inclusive SLAC data (hence also referred to as "Bloom-Gilman duality"), the structure functions in the resonance region are found on average to equal the structure functions measured in the "scaling" region at higher W. The resonance data oscillate around the scaling curve and slide along it with increasing Q^2, as seen in Fig. 2 (left).

The early F_2^p data from SLAC were extracted from cross sections assuming a fixed value for R (= 0.18), and with a scaling curve parametrizing the limited data available in the early 1970's [38]. Since the original measurements, the F_2^p structure function has become one of the best studied quantities in lepton scattering, with data from laboratories around the world contributing to a global data base spanning over five orders of magnitude in both x and Q^2. With the advent of the Jefferson Lab data, precise F_2^p measurements now also exist in the resonance region up to $Q^2 \approx 8$ GeV^2, allowing many new aspects of duality to be quantified for the first time [39].

While the early duality studies considered only the F_2 structure function [37], Jefferson Lab experiments have in addition revealed the presence of duality in other observables. For example, Fig. 3 shows new LT-separated data from Jefferson Lab experiment E94-110 for the proton transverse (F_1^p) and longitudinal (F_L^p) structure functions in the nucleon resonance region [18]. LT-separated data from SLAC, predominantly in the DIS region, are also shown for comparison [42]. Where they refer to the same kinematic values, the Jefferson Lab and SLAC data are in excellent agreement, providing confidence in the achievement of the demanding precision required of this type of experiment. In all cases, the resonance and DIS data merge smoothly with one another in both x and Q^2.

The availability of leading twist PDF-based global fits [4, 5, 6, 7, 9] allows comparison of the resonance region data with leading twist structure functions at the same x and Q^2. The resonance data on the F_1 and F_L structure functions are also found to oscillate around the perturbative QCD (pQCD) curves, down to Q^2 as low as 0.7 GeV^2. Because most of the data lie at large values of x and small Q^2, it is vital for tests of duality to account for the effects of kinematical target mass corrections [15], which give large contributions as $x \to 1$ [16].

Table 1. Listing of Jefferson Lab unpolarized inclusive and semi-inclusive electron-nucleon scattering experiments.

Experiment	Hall	Target	Observable	Reference	Status
E94-110	C	p	R in resonance region	[18, 27, 28, 29]	data taken in 1999, analysis completed
E99-118	C	p, d	nuclear dependence of R at low Q^2	[30]	data taken in 2000, analysis completed
CLAS	B	p, d	inclusive cross sections	[25, 31]	e1/e2 run periods
E00-002	C	p, d	F_2 at low Q^2	[20]	data taken in 2003, analysis completed, pub. in progress
E00-108	C	p, d	semi-inclusive $\pi^{\pm}$ electroproduction	[32, 33]	data taken in 2003, analysis completed
E00-116	C	p, d	inclusive resonance region cross sections at intermediate Q^2	[19]	data taken in 2003, analysis completed
E02-109	C	d	R in resonance region	[34]	data taken in 2005, analysis in progress
E03-012 (BoNuS)	B	$d(n)$	neutron F_2^n via spectator tagging	[35]	data taken in 2005, analysis completed, pub. in progress
E06-009	C	d	R in resonance region & beyond: extension of E02-109 to $Q^2 = 4$ GeV^2	[36]	data taken in 2007, analysis in progress

This is clear from Fig. 3, where the data are compared with leading twist structure functions computed from PDFs to next-to-next-to-leading order (NNLO) accuracy from Alekhin [40] and MRST [41, 43]. The latter are shown with (solid) and without (dotted) target mass corrections, and clearly demonstrate the importance of subleading $1/Q^2$ effects at large x. In particular, TMCs give additional strength at large x observed in the data, which would be significantly underestimated by the leading twist functions without TMCs.

The phenomenological results raise the question of how can a scaling structure function be built up entirely from resonances, each of whose contribution falls rapidly with Q^2 [44]? A number of studies using various models have demonstrated how sums over resonances can indeed yield a Q^2 independent function (see Ref. [39] for a review). The key observation is that while
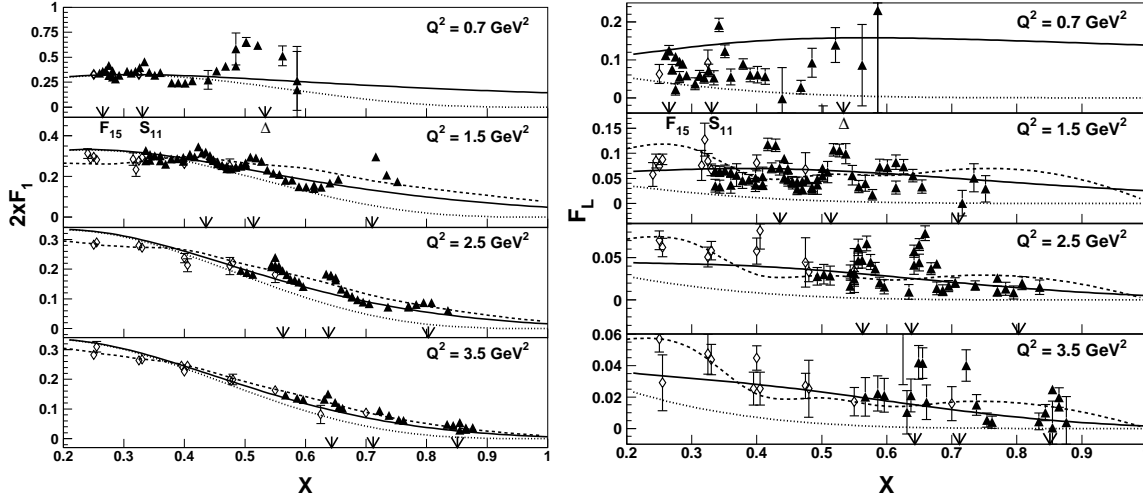
Figure 3. Purely transverse *(left)* and longitudinal *(right)* proton structure functions $2xF_1$ and F_L in the resonance region [18] (triangles), compared with earlier data from SLAC (squares). The curves are leading twist structure functions computed at NNLO from Alekhin (dashed) [40] and MRST [41] with (solid) and without (dotted) target mass corrections. The prominent resonance regions (Δ, S_{11}, F_{15}) are indicated by the arrows along the abscissa.

the contribution from each individual resonance diminishes with Q^2, with increasing energy new states become accessible whose contributions compensate in such a way as to maintain an approximately constant strength overall. At a more microscopic level, the critical aspect of realizing the suppression of the higher twists is that at least one complete set of even and odd parity resonances must be summed over for duality to hold [45]. For an explicit demonstration of how this cancellation takes place in the SU(6) quark model and its extensions, see Refs. [45, 46, 47].

3.2. Structure function moments

The degree to which quark-hadron duality holds can be more precisely quantified by computing integrals of the structure functions over x in the resonance region at fixed Q^2 values, $\int_{x_{\rm th}}^{x_{\rm res}} dx\ F_2(x, Q^2)$, where $x_{\rm th}$ corresponds to the pion production threshold at fixed Q^2, and $x_{\rm res} = Q^2/(W_{\rm res}^2 - M^2 + Q^2)$ indicates the x value at the same Q^2 where the traditional delineation between the resonance and DIS regions at $W = W_{\rm res} \equiv 2$ GeV is made. These integrals can then be compared to the corresponding integrals of the structure functions fitted to the higher-W, deep-inelastic data, at the same Q^2 and over the same interval of x. The early phenomenological findings [26] suggested that the integrated strength of the resonance structure functions above $Q^2 \approx 1$ GeV^2 was indeed very similar to that in the deep-inelastic region, including in each of the individual prominent resonance regions. In this section we explore the duality between the resonance and deep-inelastic structure functions in the context of QCD moments.

According to De Rujula, Georgi and Politzer [48], one can formally relate the appearance of quark-hadron duality to the vanishing suppression of higher twist matrix elements in the QCD moments of the structure functions [14]. Namely, if certain moments of structure functions are observed to be independent of Q^2, as implied by duality, then from Eq. (11) the moments must be dominated by the leading, Q^2 independent term, with the $1/Q^{\tau-2}$ higher twist terms suppressed. Duality is then synonymous with the suppression of higher twists, which in partonic language corresponds to the suppression, or cancellation, of interactions between the scattered

quark and the spectator system such as those illustrated in Fig. 1 (b) and (c). Conversely, if the moments display power-law Q^2 dependence, then this implies violation of duality; moreover, if the violation is not overwhelming, the Q^2 dependence of the data can be used to extract information on the higher twist matrix elements [49].
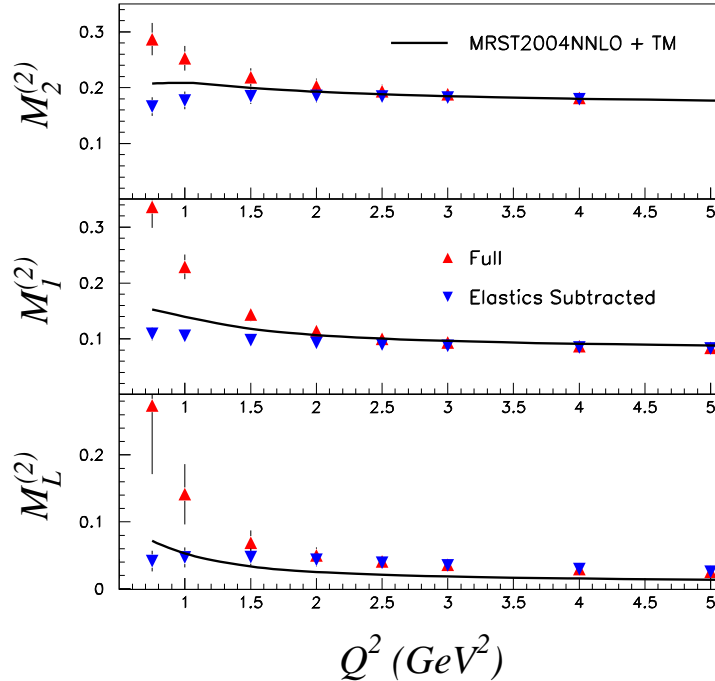

Figure 4. Total $n = 2$ moments of the proton F_2^p *(top)*, F_1^p *(center)* and F_L^p *(bottom)* structure functions determined from global fits to existing DIS data and Jefferson Lab resonance region data [50], compared with moments computed from the leading twist PDFs from MRST at NNLO [41].

The first determination [51] of the F_2^p moments from Jefferson Lab data was made utilizing structure functions measured in Hall C [26], while a later evaluation [25] included the large body of additional data from CLAS. More recently, the extraction of F_2^p has been further enhanced by LT-separated data from Hall C, shown in Fig. 2 along with the fit [24] to the LT separated cross sections. The $n = 2$ moments for the proton F_2^p, F_1^p, and F_L^p structure functions are shown in Fig. 4 versus Q^2, as determined from integrating this fit. For F_2^p they are found to be in very good agreement with the earlier measurements. Also shown is the leading-twist contribution calculated from the MRST parameterization [41], corrected for target mass effects [15].

One of the most striking features of the results in Fig. 4 is that the elastic-subtracted moments exhibit the same Q^2 dependence as the PDF fits down to $Q^2 \approx 1$ GeV^2. Even with the elastic contribution included, which vanishes in the Bjorken limit and is hence pure higher twist, there is excellent agreement between the resonance and DIS data for $Q^2 \gtrsim 2$ GeV^2. Until very recently [6, 9], this fact has not been widely appreciated or utilized in global PDF fitting efforts [4, 5], which typically impose cuts on data of $Q^2 \gtrsim 4$ GeV^2 and $W^2 \gtrsim 12$ GeV^2.

While the OPE provides a systematic approach to identifying and classifying higher twists, it does not reveal *why* these are small or *how* duality is realized globally and locally. To further explore the *local* aspects of duality within a perturbative QCD context, a ground-breaking new

approach using "truncated" moments of structure functions, developed recently by Forte *et al.* [52] and extended by Kotlorz & Kotlorz [53], was applied by Psaker *et al.* [54] to Jefferson Lab data. The virtue of truncated moments is that they obey a similar set of Q^2 evolution equations as those for PDFs themselves, which therefore enables a rigorous connection to be made between local duality and QCD. It allows one to quantify the higher twist content of various resonance regions, and determine the degree to which individual resonances are dominated by the leading twist components.

Defining the n-th truncated moment $\mathcal{M}_n$ of a PDF $q(x, Q^2)$ between $x_{\min}$ and $x_{\max}$ as

$$\mathcal{M}_n(x_{\min}, x_{\max}, Q^2) = \int_{x_{\min}}^{x_{\max}} dx\ x^{n-1}\ q(x, Q^2)\ , \tag{13}$$

the evolution equations for the truncated moments can be written as

$$\frac{d\mathcal{M}_n}{dt} = \frac{\alpha_s(Q^2)}{2\pi} \left(P_n' \otimes \mathcal{M}_n\right)\ , \quad t = \ln\left(Q^2/\Lambda_{\text{QCD}}^2\right)\ . \tag{14}$$

The symbol $\otimes$ denotes the Mellin convolution of the truncated moment and the "splitting function" P_n', which is related to the usual DGLAP evolution splitting function P [55] by $P_n'(z, \alpha_s(Q^2)) = z^n\ P(z, \alpha_s(Q^2))$. The extent to which nucleon structure function data in specific regions in x (or W) are dominated by leading twist can be determined by constructing empirical truncated moments and evolving them to different Q^2. Deviations of the evolved moments from the experimental data at the new Q^2 then reveal any higher twist contributions in the original data.

A next-to-leading order (NLO) analysis [54] of data on the proton F_2^p structure function from Jefferson Lab covering a range in Q^2 from 1 GeV^2 to ≈ 6 GeV^2 revealed intriguing behavior of the higher twists for different nucleon resonance regions. Assuming that F_2^p data beyond a large enough Q^2 (taken to be $Q^2 = Q_0^2 = 25$ GeV^2 in Ref. [54]) are dominated by leading twist, the truncated moments were computed at Q_0^2 and evolved to lower Q^2. Note that the truncated moments are computed over the range $W_{\text{th}} \leq W \leq W_{\max}$, where the $W_{\text{th}} = M + m_\pi$ is the inelastic threshold. At $Q^2 = 1$ GeV^2 this corresponds to the integration range $x_{\min} \leq x \leq x_{\text{th}}$, where $x_{\text{th}} = [1 + m_\pi(m_\pi + 2M)/Q^2]^{-1} \simeq 0.78$.

The ratio of the truncated moments of the data to the leading twist is shown in Fig. 5(a) as a function of $W_{\max}$ at $Q^2 = 1$ GeV^2, with and without target mass corrections. Including the effects of TMCs, the leading twist moment differs from the data by $\sim 15\%$ for $W_{\max} > 1.5$ GeV. To quantify the higher twist content of the specific resonance regions, and at different values of Q^2, several intervals in W are considered: $W_{\text{th}}^2 \leq W^2 \leq 1.9$ GeV^2 ($\Delta(1232)$ or first resonance region); $1.9 \leq W^2 \leq 2.5$ GeV^2 ($S_{11}(1535)$ or second resonance region); and $2.5 \leq W^2 \leq 3.1$ GeV^2 ($F_{15}(1680)$ or third resonance region). The higher twist contributions to $\mathcal{M}_2$ in these regions are shown in Fig. 5(b) as ratios to moments of the data.

The results indicate deviations from leading twist behavior of the entire resonance region data (filled circles in Fig. 5(b)) at the level of $\lesssim 15\%$ for all values of Q^2 considered, with significant Q^2 dependence for $Q^2 \lesssim 4$ GeV^2. The strong Q^2 dependence of the higher twists is evident here in the change of sign around $Q^2 = 2$ GeV^2, with the higher twists going from $\approx -10\%$ at $Q^2 = 1$ GeV^2 to ≈ 10–15% for $Q^2 \sim 3 - 6$ GeV^2. At larger Q^2 the higher twists are naturally expected to decrease, once the leading twist component of the moments begins to dominate.

Interestingly, the magnitude of the higher twist contributions in the Δ region (diamonds) is smallest, decreasing from $\approx -15\%$ of the data at $Q^2 = 1$ GeV^2 to values consistent with zero at larger Q^2. The higher twists are largest, on the other hand, for the S_{11} region (squares), where they vary between $\approx -15\%$ of the data at $Q^2 = 1$ GeV^2 and 20–25\% at $Q^2 \sim 5$ GeV^2. Combined, the higher twist contribution from the first two resonance regions (dotted curve) is
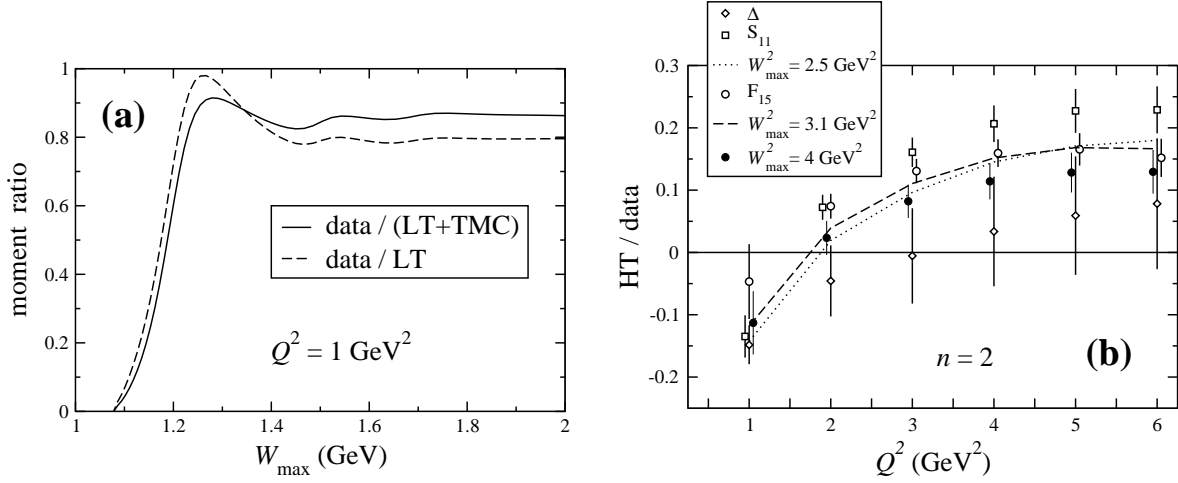
Figure 5. (a) Ratio of the $\mathcal{M}_2$ truncated moments of the data to the leading twist + TMC (solid), and data to leading twist without TMC (dashed) at $Q^2 = 1$ GeV^2, as a function of $W_{\max}$. (b) Q^2 dependence of the fractional higher twist (HT) contribution to the $n = 2$ truncated moment data, for various intervals in W.

$\lesssim 15\%$ in magnitude for all Q^2. The rather dramatic difference between the Δ and the S_{11}, may, at least in part, be due to the choice of the differentiation point of $W^2 = 1.9$ GeV^2. A lower W^2 choice, for instance, would lower the higher twist content of the S_{11} at large Q^2, while raising that of the Δ. However, this W^2 choice corresponds to the local minimum between these two resonances in the inclusive spectra, and is the one most widely utilized.

The higher twist content of the F_{15} region (open circles) is similar to the S_{11} at low Q^2, but decreases more rapidly for $Q^2 > 3$ GeV^2. The higher twist content of the first three resonance regions combined (dashed curve) is $\lesssim 15$–20% in magnitude for $Q^2 \leq 6$ GeV^2. Integrating up to $W^2_{\max} = 4$ GeV^2 (filled circles), the data on the $n = 2$ truncated moment are found to be leading twist dominated at the level of 85–90% over the entire Q^2 range.

The results in Fig. 5 can be compared with quark model expectations [45, 46], which predict systematic deviations of resonance data from local duality. Assuming dominance of magnetic coupling, the proton data are expected to overestimate the DIS function in the second and third resonance regions due to the relative strengths of couplings to odd-parity resonances; the positive higher twists observed in Fig. 5(b) for $Q^2 \gtrsim 2$ GeV^2 indeed support these predictions.

4. Deuteron F_2 measurements

Together with hydrogen, inclusive lepton scattering from deuterium targets has provided an extensive data base of F_2 structure function measurements over a large range of kinematics. While a significant quantity of F_2^d data was collected from experiments at CERN and SLAC, the quasi-elastic and nucleon resonance regions, especially at low and moderate Q^2 ($\approx$ few GeV^2), were only mapped precisely with the advent of Jefferson Lab data [26, 31]. Similarly, Jefferson Lab contributed with precision F_2^d data in the region of $x > 1$ [56], of relevance for constructing higher moments of deuteron structure functions.

Experiments in Hall C [26, 56] have provided F_2^d data in select regions of x and Q^2, while inclusive cross section measurements in CLAS have covered a continuous two-dimensional region over the entire resonance region up to $Q^2 = 6$ GeV^2. This combination is rather useful for determining moments of F_2. In such extractions one usually assumes that the ratio R for the deuteron is similar to that for the proton at scales Q^2 of a few GeV^2 [57]. New measurements

which will test this assumption will be reviewed in Sec. 6.

Table 2. Lowest two moments (for $n = 2$ and 4) of the isovector F_2 structure function. Experimental results for $Q^2 \approx 4$ GeV^2 are compared with lattice calculations extrapolated to the chiral limit.

n	Niculescu *et al.* [58] (Hall C)	Osipenko *et al.* [59] (Hall B)	Detmold *et al.* [60] (lattice)
2	0.049(17)	0.050(9)	0.059(8)
4	0.015(3)	0.0094(16)	0.008(3)

The results of the moment analyses are shown in Table 2, expressed as the isovector (proton minus neutron) combination, and compared with isovector moments from lattice QCD [60, 61]. For simplicity the neutron moments here are defined as the difference between the deuteron and proton moments — see, however, Sec. 5.1 below. The $n = 2$ moments from the Hall B [59] and Hall C [58] analyses agree well with each other, and with the lattice extraction, which includes the effects of pion loops and the intermediate $\Delta(1232)$ resonance in the chiral extrapolation. For the $n = 4$ moment the comparison between the Hall B and Halls C results shows a slight discrepancy, which may be reduced once precision high-x data at $Q^2 \sim 4$ GeV^2 are included in the extractions.

Analysis of the Q^2-dependence of the deuteron F_2 moments in Ref. [31] suggests a partial cancellation of different higher twist contributions entering in the OPE with different signs, which is one of the manifestations of quark-hadron duality. The slow variation with Q^2 of the structure function moments, down to $Q^2 \approx 1$ GeV^2, was also found in the analysis of proton data [51], where such cancellations were found to be mainly driven by the elastic contribution. Furthermore, by comparing the proton and (nuclear corrected) neutron structure function moments, the higher twist contributions were found to be essentially isospin independent [62]. This suggests the possible dominance of ud correlations over uu and dd in the nucleon, and implies higher twist corrections that are consistent with zero in the isovector F_2 structure function.

More recently, high precision deuteron cross sections in the resonance region have been measured in Hall C [34, 36] with the aim of providing LT separated deuteron structure functions of comparable precision and kinematic coverage to those performed for the proton. These higher precision LT separated data will allow for a significant further reduction in the uncertainties in the current nonsinglet F_2 extractions.

5. Neutron F_2 structure function

A complete understanding of the valence quark structure of the nucleon requires knowledge of both its u and d quark distributions. While the u distribution is relatively well constrained by measurements of the proton F_2^p structure function, in contrast the d quark distribution is poorly determined due to the lack of comparable data on the neutron structure function F_2^n. The absence of free neutron targets makes it necessary to use light nuclei such as deuterium as effective neutron targets, and one must therefore deal with the problem of extracting neutron information from nuclear data.

5.1. Neutron structure from inclusive F_2 data

In standard global PDF analyses, sensitivity to the d-quark from charged lepton scattering is primarily provided by the neutron in the deuteron. Usually the neutron F_2^n structure function

is extracted by subtracting the deuteron and proton structure function data assuming that nuclear corrections are negligible. At large x, however, the ratio of the deuteron to free nucleon structure functions is predicted to deviate significantly from unity [63, 64, 65, 66], which can have significant impact on the behavior of the extracted neutron structure function at large x [9, 67].

Even when nuclear effects are considered, there exist practical difficulties with extracting information on the free neutron from nuclear data, especially in the nucleon resonance region, where resonance structure is largely smeared out by nucleon Fermi motion. A recent analysis [68] used a new method [66] to extract F_2^n from F_2^d and F_2^p data, in which nuclear effects are parameterized via an additive correction to the free nucleon structure functions, in contrast to the more common multiplicative method [69] which fails for functions with zeros or with non-smooth data. In the standard impulse approximation approach to nuclear structure functions, the deuteron structure function can be written as a convolution [65, 66]

$$F_2^d(x, Q^2) = \sum_{N=p,n} \int dy \ f_{N/d}(y, \rho) \ F_2^N(x/y, Q^2), \qquad (15)$$

where $f_{N/d}$ is the light-cone momentum distribution of nucleons in the deuteron (or "smearing function"), and is a function of the momentum fraction y of the deuteron carried by the struck nucleon, and of the virtual photon "velocity" ρ (see Eq. (4)). The smearing function encodes the effects of the deuteron wave function, accounting for nuclear Fermi motion and binding effects, as well as kinematical finite-Q^2 corrections. Although not well constrained, nucleon off-shell effects have also been studied [63, 64, 65]; their influence appears to be small compared with the errors on the existing data, except at very large x.
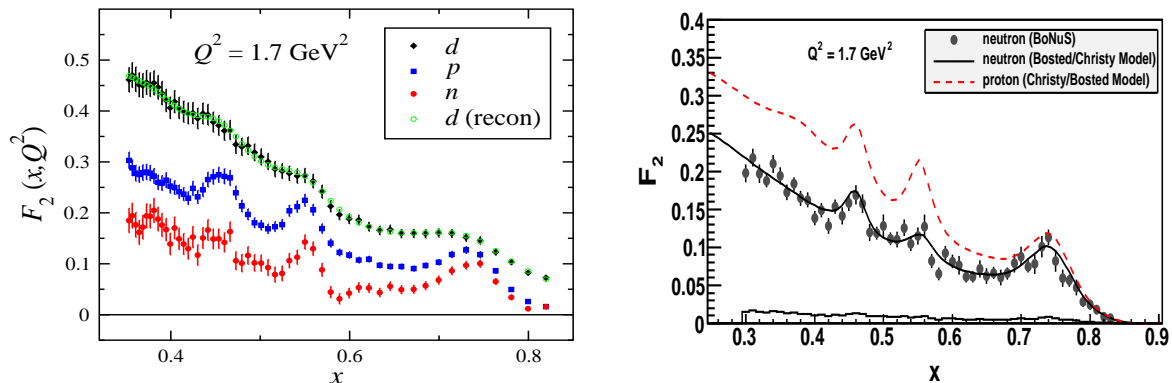

Figure 6. *(Left)* Neutron F_2^n structure function extracted from inclusive deuteron and proton data at $Q^2 = 1.7$ GeV^2 [68], together with the reconstructed F_2^d. *(Right)* Neutron structure function extracted from the BoNuS experiment [35], compared with the Bosted/Christy model of the neutron F_2^n [70] and the corresponding Christy/Bosted parametrization for F_2^p [24].

In Fig. 6 we illustrate the results of a typical extraction of F_2^n from Jefferson Lab F_2^d and F_2^p data at $Q^2 = 1.7$ GeV^2. The proton data show clear resonant structure at large x, which is mostly washed out in the deuteron data. The resulting neutron F_2^n is shown after two iterations of the procedure with an initial guess of $F_2^n = F_2^p$. Clear neutron resonance structure is visible in the first (Δ) and second resonance regions, at $x \sim 0.75$ and 0.55, respectively, with some

structure visible also in the third resonance region at $x \sim 0.45$, albeit with larger errors. The deuteron F_2^d reconstructed from the proton and extracted neutron data via Eq. (15) indicates the relative accuracy and self-consistency of the extracted F_2^n.

Of course it is not possible to avoid nuclear model dependence in the inversion procedure, and some differences in the extracted F_2^n will arise using different models for the smearing functions $f_{N/d}$. To remove, or at least minimize, the model dependence in the extracted free neutron structure, several methods have been proposed, such as utilizing inclusive DIS from $A = 3$ mirror nuclei [71, 72, 73], and semi-inclusive DIS from a deuteron with spectator tagging [35, 74]. In addition, experiments involving weak interaction probes [75, 76, 77] can provide the information on the flavor separated valence quark distributions directly. In the next section we discuss in detail one of these methods for determining the free neutron structure, namely the BoNuS experiment at Jefferson Lab [35].

5.2. Tagged neutron structure functions

To overcome the absence of free neutron targets, the Hall B BoNuS (Barely Off-shell NeUtron Structure) experiment has measured inclusive electron scattering on an almost free neutron using the CLAS spectrometer and a recoil detector to tag low momentum protons. The protons are tracked in a novel radial time projection chamber [78] utilizing gas electron multiplier foils to amplify the proton ionization in a cylindrical drift region filled with a mixture of Helium and Di-Methyl Ether, and with the proton momentum determined from the track curvature in a solenoidal magnetic field. Slow backward-moving spectator protons are tagged with momenta as low as 70 MeV in coincidence with the scattered electron in the reaction $D(e, e'p_s)X$. This technique ensures that the electron scattering took place on an almost free neutron, with its initial four-momentum inferred from the observed spectator proton. Cutting on spectator protons with momenta between 70 and 120 MeV and laboratory angles greater than 120 degrees minimizes the contributions from final state interactions and off-shell effects to less than several percent on the extracted neutron cross section.

While inclusive scattering from deuterium results in resonances which are significantly broadened (often to the point of being unobservable), determination of the initial neutron momentum allows for a dramatic reduction in the fermi smearing effects and results in reconstructed resonance widths comparable to the inclusive proton measurements. In addition, the large CLAS acceptance for the scattered electron allowed for the tagged neutron cross section to be measured over a significant kinematic range in both W^2 and Q^2 at beam energies of 4.2 GeV and 5.3 GeV. BoNuS F_2^n data extracted at a beam energy of 5.3 GeV and $Q^2 = 1.7$ GeV^2 are shown in Fig. 6 (right panel) for x values from pion production threshold through the resonance region and into the DIS regime. This will allow for the first time a unambiguous study of the inclusive neutron resonance structure functions.

An extension of BoNuS has been approved [79] to run at a beam energy of 11 GeV after the energy upgrade of the CEBAF accelerator. The kinematic coverage will allow the extraction of the ratio of neutron to proton structure functions F_2^n/F_2^p to x as large as 0.8, and the corresponding d to u large x parton distribution ratio. Other quantities which BoNuS will make possible to measure include the elastic neutron form factor, quark-hadron duality on the neutron, semi-inclusive DIS and resonance production channels, hard exclusive reactions such as deeply-virtual Compton scattering or deeply-virtual meson-production from the neutron, as well as potentially the inclusive structure function of a virtual pion.

6. Longitudinal structure function F_L

The unpolarized inclusive proton cross section contains two independent structure functions. While F_2^p has been measured to high precision over many orders of magnitude in both x and Q^2, measurements of the longitudinal structure function F_L^p (and the ratio R) have been

significantly more limited in both precision and kinematic coverage. This is due in part to the challenges inherent in performing LT separations, which typically require point-to-point systematic uncertainties in ϵ to be smaller than 2% to obtain uncertainties on F_L of less than 20%.

While the inclusive cross section is proportional to $2xF_1 + \epsilon F_L$, the F_2 structure function $\sim 2xF_1 + F_L$, so that F_2 is only proportional to the cross section for $\epsilon = 1$. At high Q^2 the scattering of longitudinal photons from spin-1/2 quarks is suppressed, and in the parton model one expects F_L (and R) to vanish as $Q^2 \to \infty$. At low Q^2, however, F_L is no longer suppressed, and could be sizable, especially in the resonance region and at large x. On the other hand, F_L is dominated by the gluon contribution at small x, where new measurements from HERA [80] have shown that it continues to rise. In the kinematic range of Jefferson Lab F_L has been found to be typically 20% of the magnitude of F_2, which is consistent with earlier SLAC measurements where the kinematic regions overlap.

An extensive program of LT separations has been carried out in Hall C, including measurements of the longitudinal strength in the resonance region for $0.3 < Q^2 < 4.5$ GeV^2 for both proton [18] and deuteron [34, 36] targets. The Jefferson Lab experiments listed in Table 1 for which LT separations have been performed for the proton or deuteron are E94-110, E99-118, E00-002, E02-109, and E06-009. The Jefferson Lab data complement well the previous results at smaller x from SLAC and NMC in this Q^2 region, and improve dramatically on the few measurements that existed below $Q^2 = 8$ GeV^2 in this x region, which had typical errors on R and F_L of 100% or more — see Fig. 7 (left).

The recent precision LT separated measurements of proton cross sections [18] have allowed for the first time detailed duality studies in all of the unpolarized structure functions and their moments. The results of the proton separated structure functions in the resonance region were presented in Fig. 3 in Sec.3. Although significant resonant strength is observed in F_L (or R), evidence of duality is nonetheless observed in this structure function, along with F_2 and F_1.

In addition to the proton data, Jefferson Lab experiment E02-109 measured the LT separated F_2 and F_L structure functions of the deuteron, in the same W^2 and Q^2 ranges, and with the same high precision as E94-110 did for the proton. This will allow quantitative studies of duality in both the longitudinal and transverse channels for the deuteron. If duality holds well for both the proton and neutron separately, it will hold to even better accuracy for the deuteron since the Fermi motion effects intrinsically perform some of the averaging over the resonances. However, if duality does not hold for the LT separated neutron structure functions, this should be observable in the deuteron data, and will thus provide a critical test for models of duality.

In addition to the resonance region, measurements of the inclusive longitudinal proton and deuteron structure have also been performed at lower x (higher W^2) and lower Q^2. While the longitudinal strength is significant at Q^2 of several GeV^2, the proton F_L structure function is constrained by current conservation to behave, for fixed W, as $F_L \sim Q^4$ for $Q^2 \to 0$. However, even with the new Jefferson Lab data, which extend down to $Q^2 = 0.15$ GeV^2 [81], the Q^2 at which this behavior sets in has not yet been observed.

Another interesting test provided by the E99-118 data is whether the relative longitudinal contribution to the cross section embodied in R is different in the deuteron and proton at these low Q^2 values. While the higher Q^2 data from SLAC and NMC exhibit no significant difference in the deuteron and proton R, the Jefferson Lab results shown in Fig. 7 (right) suggest a possible suppression of R in the deuteron relative to the proton for $Q^2 < 1$ GeV^2. Although this suppression is consistent with the two lowest Q^2 data points from SLAC, the uncertainties are dominated by systematic errors and the combined significance of the effect is still less than $2\,\sigma$. Conclusive experimental evidence for the possible suppression of R in deuterium at low Q^2 will likely be provided when the results from additional data from E00-002 are finalized in very near future.
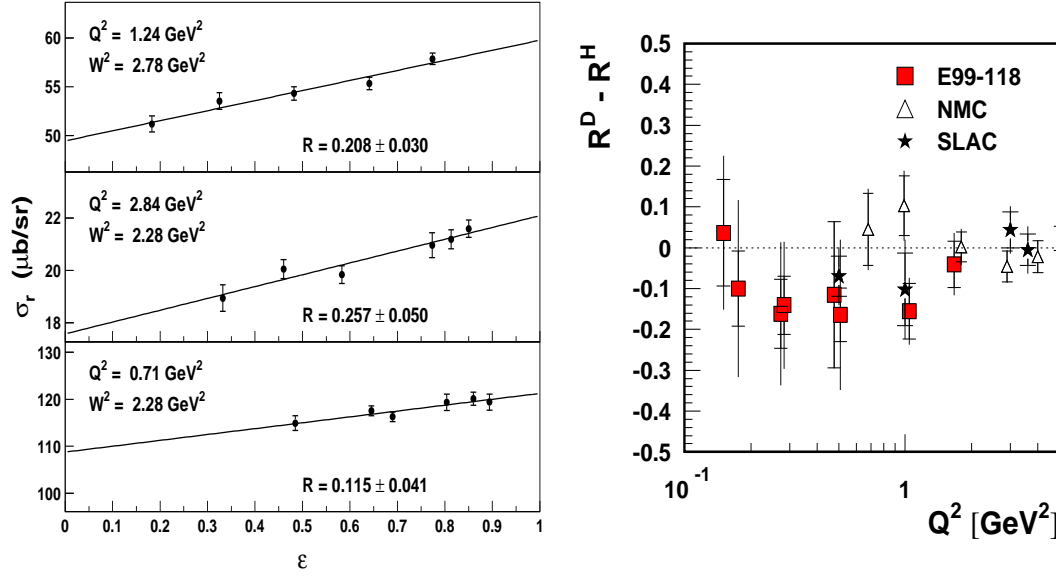
Figure 7. *(Left)* Sample LT separations from Jefferson Lab experiment E94-110 [18]. *(Right)* Difference between the ratios R in deuterium and hydrogen versus Q^2, from E99-118 [81], compared with previous NMC and SLAC measurements.

7. Semi-inclusive deep inelastic scattering

In addition to the traditional F_2 and F_L structure function observables, a number of other processes have been studied at Jefferson Lab over the past decade, with potentially important consequences for our understanding of the workings of QCD at low energy. In this section we focus on semi-inclusive pion electroproduction.

An analysis of the semi-inclusive process $e\,N \rightarrow e\,h\,X$, where a hadron h is detected in the final state in coincidence with the scattered electron, has recently been made using data from Hall C in the resonance–scaling transition region [32, 33]. One of the main motivations for studying semi-inclusive meson production is the promise of flavor separation via tagging of specific mesons in the final state. In the valence quark region a produced π^+ (π^-) meson, for example, primarily results from scattering off a u (d) quark in the proton.

The semi-inclusive cross section at LO in α_s is given by a simple product of quark distribution and quark $\rightarrow$ hadron fragmentation functions,

$$\frac{d\sigma}{dxdz} \;\sim\; \sum_q e_q^2\, q(x)\, D_q^h(z) \;\equiv\; \mathcal{N}_N^h(x,z)\,. \tag{16}$$

Here the fragmentation function $D_q^h(z)$ gives the probability for a quark q to fragment to a hadron h with a fraction $z = p_h \cdot p/q \cdot p = E_h/\nu$ of the quark's (or virtual photon's) laboratory frame energy. Although at LO the scattering and particle production mechanisms are independent, higher order pQCD corrections give rise to non-factorizable terms, which involve convolutions of the PDFs and fragmentation functions with hard coefficient functions [82].

For hadrons produced collinearly with the virtual photon, the invariant mass W' of the undetected hadronic system X at large Q^2 can be written [83] $W'^2 \approx M^2 + Q^2(1-z)(1-x)/x$, where the hadron mass is neglected with respect to Q^2. In the elastic limit, $z \rightarrow 1$, the hadron carries all of the photon's energy (with $W' \rightarrow M$), so z is also referred to as the "elasticity".

While formally the LO factorized expression for the cross section (16) may be valid at large Q^2, at finite Q^2 there are important corrections arising from the finite masses of the target and produced hadron. One can show, however, that the LO factorization holds even at finite Q^2, provided the parton distribution and fragmentation functions are expressed in terms of generalized scaling variables [84], $q(x)D_q^h(z) \to q(\xi_h)D_q^h(\zeta_h)$, where $\zeta_h = (z_h\xi/2x)(1 + \sqrt{1 - 4x^2M^2m_{h\perp}^2/z^2Q^4})$ and $\xi_h = \xi(1 + m_h^2/\zeta_h Q^2)$, with $m_{h\perp}^2 = m_h^2 + p_{h\perp}^2$. Not surprisingly, these effects become large at large x and z when Q^2 is small; however, for heavier produced hadrons such as kaons or protons, significant effects can also arise at small values of z [84].

The validity of the factorized hypothesis in Eq. (16) relies on the existence of a sufficiently large gap in rapidity $\eta = \ln\left[(E_h - p_h^z)/(E_h + p_h^z)\right]/2$ to allow a clean separation of the current fragmentation region (hadrons produced from the struck quark) from the target fragmentation region (hadrons produced from the spectator quark system). At high energies a gap of $\Delta\eta \approx 2$, which is typically required for a clean separation [85], can be achieved over a large range of z; at low energies, however, this can only be reached at larger values of z. On the other hand, at fixed x and Q^2 the large-z region corresponds to resonance dominance of the undetected hadronic system X (corresponding to small W'), so that the factorized description in terms of partonic distributions must eventually break down. It is vital therefore to establish empirically the limits beyond which the simple x and z factorization of Eq. (16) is no longer valid.

It is intriguing in particular to observe whether W' can play a role analogous to W for duality in inclusive scattering, when the undetected hadronic system X is dominated by resonances $W' \lesssim 2$ GeV. In terms of hadronic variables the fragmentation process can be described through the excitation of nucleon resonances, N^*, and their subsequent decays into pions (or other mesons) and lower-lying resonances, N'^*. The hadronic description must be rather elaborate, however, as the production of fast outgoing pions in the current fragmentation region at high energy requires nontrivial cancellations of the angular distributions from various decay channels [44, 45, 86],

$$\mathcal{N}_N^h(x,z) = \sum_{N'^*}\left|\sum_{N^*} F_{\gamma^*N\to N^*}(Q^2,W^2)\,\mathcal{D}_{N^*\to N'^*h}(W^2,W'^2)\right|^2 \tag{17}$$

where $F_{\gamma^*N\to N^*}$ is the $N \to N^*$ transition form factor, which depends on the masses of the virtual photon and excited nucleon ($W = M_{N^*}$), and $\mathcal{D}_{N^*\to N'^*h}$ is a function representing the decay $N^* \to N'^*h$.

A dedicated experiment (E00-018) to study duality in $\pi^\pm$ electroproduction was performed in Hall C [32, 33], in which a 5.5 GeV electron beam was scattered from proton and deuteron targets at Q^2 between 1.8 and 6.0 GeV^2, for $0.3 \le x \le 0.55$, with z in the range $0.35 - 1$. From the deuterium data the ratio of unfavored to favored fragmentation functions D^-/D^+ was constructed, where D^+ corresponds to a pion containing the struck quark ($e.g.$, π^+ from a struck u or $\bar{d}$ quark), while D^- describes the fragmentation of a quark not contained in the valence structure of the pion ($e.g.$, a d quark for the π^+). Since at moderate x the dependence on PDFs cancels, the fragmentation function ratio is approximately given by $D^-/D^+ = (4 - \mathcal{N}_d^{\pi^+}/\mathcal{N}_d^{\pi^-})/(4\mathcal{N}_d^{\pi^+}/\mathcal{N}_{\lceil}^{\pi^-} - 1)$, where $\mathcal{N}_d^\pi$ is the yield of produced pions in Eq. (17).

The Jefferson Lab data for D^-/D^+ from E00-108 are shown in Fig. 8 as a function of z at fixed $x = 0.32$ and $Q^2 = 2.3$ GeV^2 [32], and compared with earlier HERMES data at higher energies [87]. Despite the different energies, there is good overall agreement between the two measurements, even though the Jefferson Lab data sit slightly higher. Furthermore, the D^-/D^+ ratio extracted from the Jefferson Lab data shows a smooth dependence on z, which is quite remarkable given that the data cover the full resonance region, $0.88 < W'^2 < 4.2$ GeV^2. This
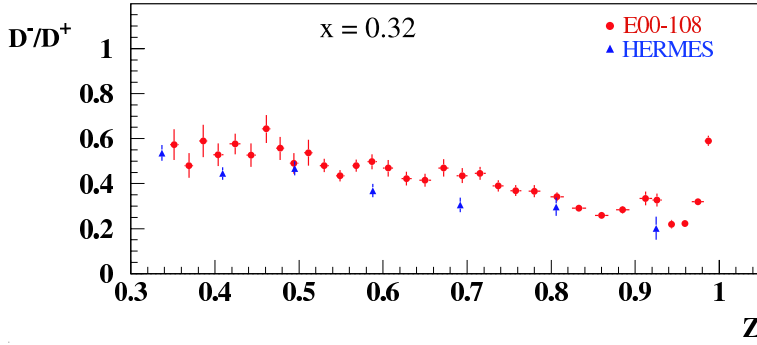
Figure 8. The ratio of unfavored to favored fragmentation functions D^-/D^+ as a function of z extracted from deuterium data, for $x = 0.32$ [32].

strongly suggests a suppression or cancellation of the resonance excitations in the π^+/π^- cross section ratio, and hence in the fragmentation function ratio.

Similar cancellations between resonances naturally arises in quark models, such as those discussed by Close *et al.* [45, 47] for the $\gamma N \to \pi^\pm N'^*$ reaction. The pattern of constructive and destructive interference, which was a crucial feature of the appearance of duality in inclusive structure functions, is also repeated in the semi-inclusive case when one sums over the states N'^*. Moreover, the smooth behavior of the fragmentation function ratio D^-/D^+ in Fig. 8 can be qualitatively understood from the relative weights of the matrix elements, which are always 4 times larger than for π^- production. In this case the resonance contributions to this ratio cancel exactly, leaving behind only the smooth background as would be expected at high energies. This may account for the striking lack of resonance structure in the resonance region fragmentation functions in Fig. 8.

8. Outlook

8.1. Impact of Jefferson Lab data

The first decade of unpolarized structure function measurements at Jefferson Lab has had significant impact on our understanding of nucleon structure, both for leading twist parton distributions and for the resonance–scaling transition and related studies of quark-hadron duality. With most of the data concentrated in the low-W region in the $Q^2 \sim$ few GeV^2 range, the greatest influence on the global data base has naturally been at large x.

Recently a new global PDF analysis was performed [9], exploring the possibility of reducing the uncertainties at large x by relaxing the constraints on the kinematics over which data are included in the fit. The data sets combined proton and deuteron DIS structure functions from Jefferson Lab, SLAC and CERN (NMC) with new ep collider data from HERA, as well as new Drell-Yan, W asymmetry and jet cross sections from pp and pd collisions at Fermilab. The new fit (referred to as "CTEQ6X") allowed for a significant increase in the large-x data set (*e.g.*, a factor of two more DIS data points) by incorporating data for $W^2 > 3$ GeV^2 and $Q^2 > 1.69$ GeV^2, lower than in the standard global fits [5, 88] which typically use $W^2 > 12.25$ GeV^2 and $Q^2 > 4$ GeV^2. The new analysis also systematically studied the effects of target mass and higher twist contributions, and realistic nuclear corrections for deuterium data.

Results from the CTEQ6X fit are shown in Fig. 9 (left) for the u and d quark PDFs, normalized to the earlier CTEQ6.1 fit, which had no nuclear or subleading $1/Q^2$ corrections applied. The biggest change is the ~ 30–40% suppression of the d quark at $x \sim 0.8$, which is found to be stable with respect to variations in the W^2 and Q^2 cuts, provided both TMC and higher twist corrections are included. The effect of the expanded data base is more dramatically
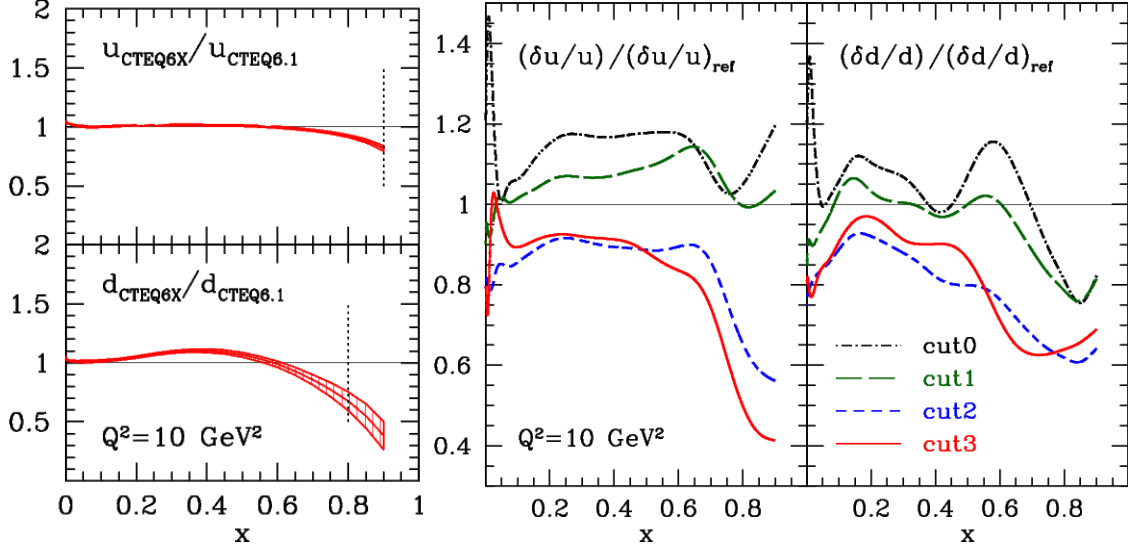
Figure 9. *(Left)* CTEQ6X fit for u and d quark PDFs, normalized to the earlier CTEQ6.1 fit [88]. The vertical lines show the approximate values of x above which PDFs are not directly constrained by data. The error bands correspond to $\Delta\chi = 1$. *(Right)* Relative errors on u and d quark PDFs, normalized to the relative errors in the reference fit.

illustrated in Fig. 9 (right), which shows the relative u and d PDF errors for a range of W and Q^2 cuts ("cut0" being the standard cut, "cut3" the more stringent CTEQ6X cut, and intermediate cuts "cut1" and "cut2"), normalized to those of a reference fit with "cut0" and no nuclear or subleading corrections. The result is a reduction of the errors by up to 40–60% at $x \gtrsim 0.7$, which will have a profound impact on applications of PDFs in high energy processes, such as those as the LHC, as well as in constraining low-energy models of quark distributions.

8.2. Future prospects

Uncertainties in PDFs will be further reduced with the availability of data at even larger x and Q^2 from Jefferson Lab after its 12 GeV energy upgrade, which will determine the d quark distribution up to $x \sim 0.8$ with minimal theoretical uncertainties associated with nuclear corrections. Several of the planned experiments include BoNuS12 [79], which will extend to larger x the earlier measurements of low-momentum, backward protons in semi-inclusive scattering from deuterium (Sec. 5.2); the MARATHON experiment [73], which plans to extract F_2^n/F_2^p from the ratio of ^{3}He to ^{3}H structure functions, in which the nuclear corrections cancel to within $\sim 1\%$ [71, 72]; and the program of parity-violating DIS measurements on hydrogen [76], which will be sensitive to a new combination of d/u in the proton, free of nuclear corrections.

In the resonance region, experiment E12-10-002 [89] will extend proton and deuteron structure function measurements up to $Q^2 \sim 17$ GeV^2 and enable tests of quark-hadron duality over a much larger kinematic range, ultimately providing stronger constraints on large-x PDFs. And finally, a new avenue for exploring nucleon structure at 12 GeV will be opened up with semi-inclusive meson production experiments [90], which will test the factorization of scattering and fragmentation subprocesses needed for a partonic interpretation of semi-inclusive cross sections. A successful program of semi-inclusive measurements tagging specific mesons in the final state would allow unprecedented access to the flavor dependence of PDFs in previously unexplored regions of kinematics.

Acknowledgments

References

 [1] W. K. H. Panofsky, in Proceedings of the 14th International Conference on High Energy Physics, Vienna, Austria (1968); E. D. Bloom *et al.*, Phys. Rev. Lett. **23**, 930 (1969); M. Breidenbach *et al.*, Phys. Rev. Lett. **23**, 935 (1969).
 [2] R. E. Taylor, in International Symposium of Lepton and Photon Interactions, Stanford (1975).
 [3] R. P. Feynman, Phys. Rev. Lett. **23**, 1415 (1969); J. D. Bjorken and E. A. Paschos, Phys. Rev. **185**, 1975 (1969).
 [4] P. M. Nadolsky *et al.*, Phys. Rev. D **78**, 013004 (2008).
 [5] A. D. Martin, W. J. Stirling, R. S. Thorne and G. Watt, Eur. Phys. J. C **63**, 189 (2009).
 [6] S. Alekhin, J. Blumlein, S. Klein and S. Moch, Phys. Rev. D **81**, 014032 (2010).
 [7] R. D. Ball *et al.*, arXiv:1101.1300 [hep-ph].
 [8] A. Levy, arXiv:hep-ph/0002015.
 [9] A. Accardi *et al.*, Phys. Rev. D **81**, 034016 (2010).
[10] O. Nachtmann, Nucl. Phys. **B63**, 237 (1973).
[11] O. W. Greenberg and D. Bhaumik, Phys. Rev. D **4**, 2048 (1971).
[12] L. N. Hand, Phys. Rev. **129**, 1834 (1963).
[13] M. N. Rosenbluth, Phys. Rev. **79**, 615 (1950).
[14] K. Wilson, Phys. Rev. **179**, 1499 (1969).
[15] H. Georgi and H. D. Politzer, Phys. Rev. D **14**, 1829 (1976).
[16] I. Schienbein *et al.*, J. Phys. G **35**, 053101 (2008).
[17] R. K. Ellis, W. Furmanski and R. Petronzio, Nucl. Phys. **B212**, 29 (1983); S. Kretzer and M. H. Reno, Phys. Rev. D **66**, 113007 (2002); A. Accardi and J. W. Qiu, JHEP **07**, 090 (2008);
[18] Y. Liang *et al.*, arXiv:nucl-ex/0410027.
[19] S. P. Malace *et al.*, Phys. Rev. C **80**, 035207 (2009).
[20] Jefferson Lab Experiment E00-002, F_2^N *at low* Q^2, C. E. Keppel and M. I. Niculescu spokespersons.
[21] L. W. Whitlow *et al.*, Phys. Lett. B **282**, 475 (1992); L. W. Whitlow, Ph.D. thesis, American University (1990).
[22] M. Arneodo *et al.*, Nucl. Phys. **B483**, 3 (1997).
[23] H. Abramowicz, E. M. Levin, A. Levy and U. Maor, Phys. Lett. B **269**, 465 (1991); H. Abramowicz and A. Levy, hep-ph/9712415.
[24] M. E. Christy and P. E. Bosted, Phys. Rev. C **81**, 055213 (2010).
[25] M. Osipenko *et al.*, Phys. Rev. D **67**, 092001 (2003).
[26] I. Niculescu *et al.*, Phys. Rev. Lett. **85** 1182, 1186 (2000).
[27] M. E. Christy *et al.*, Phys. Rev. C **70**, 015206 (2004).
[28] V. Tvaskis *et al.*, Phys. Rev. C **73**, 025206 (2006).
[29] Y. Liang, M. E. Christy, R. Ent and C. E. Keppel, Phys. Rev. C **73**, 065201 (2006).
[30] V. Tvaskis *et al.*, Phys. Rev. Lett. **98**, 142301 (2007).
[31] M. Osipenko *et al.*, Phys. Rev. C **73**, 045205 (2006).
[32] T. Navasardyan *et al.*, Phys. Rev. Lett. **98**, 022001 (2007).
[33] H. Mkrtchyan *et al.*, Phys. Lett. B **665**, 20 (2008).
[34] V. Tvaskis, J. Steinman and R. Bradford, Nucl. Phys. Proc. Suppl. **159**, 163 (2006).
[35] Jefferson Lab Experiment E03-012, *The structure of the free neutron via spectator tagging*, H. C. Fenker, C. E. Keppel, S. Kuhn, and W. Melnitchouk spokespersons.
[36] Jefferson Lab Experiment E06-009, *Measurement of* $R = \sigma_L/\sigma_T$ *on deuterium in the nucleon resonance region and beyond*, M. E. Christy and C. E. Keppel spokespersons.
[37] E. D. Bloom and F. J. Gilman, Phys. Rev. Lett. **25**, 1140 (1970); Phys. Rev. D **4**, 2901 (1971).
[38] G. Miller *et al.*, Phys. Rev. D **5**, 528 (1972).
[39] W. Melnitchouk, R. Ent and C. E. Keppel, Phys. Rep. **406**, 127 (2005).
[40] S. Alekhin, Phys. Rev. D **68**, 014002 (2003).
[41] A. D. Martin, R. G. Roberts, W. J. Stirling and R. S. Thorne, Phys. Lett. B **604**, 61 (2004).
[42] S. Dasu *et al.*, Phys. Rev. D **49**, 5641 (1994).
[43] A. D. Martin, R. G. Roberts, W. J. Stirling and R. S. Thorne, Eur. Phys. J. C **4**, 463 (1998).

[44] N. Isgur, S. Jeschonnek, W. Melnitchouk and J. W. Van Orden, Phys. Rev. D **64**, 054005 (2001).

[45] F. E. Close and N. Isgur, Phys. Lett. B **509**, 81 (2001).

[46] F. E. Close and W. Melnitchouk, Phys. Rev. C **68**, 035210 (2003).

[47] F. E. Close and W. Melnitchouk, Phys. Rev. C **79**, 055202 (2009).

[48] A. De Rujula, H. Georgi and H. D. Politzer, Annals Phys. **103**, 315 (1977).

[49] X. D. Ji and P. Unrau, Phys. Rev. D **52**, 72 (1995).

[50] M. E. Christy *et al.*, unpublished (2004).

[51] C. S. Armstrong *et al.*, Phys. Rev. D **63**, 094008 (2001).

[52] S. Forte and L. Magnea, Phys. Lett. B **448**, 295 (1999); S. Forte, L. Magnea, A. Piccione and G. Ridolfi, Nucl. Phys. **B594**, 46 (2001); A. Piccione, Phys. Lett. B **518**, 207 (2001).

[53] D. Kotlorz and A. Kotlorz, Phys. Lett. B **644**, 284 (2007).

[54] A. Psaker, W. Melnitchouk, M. E. Christy and C. Keppel, Phys. Rev. C **78**, 025206 (2008).

[55] V. N. Gribov and L. N. Lipatov, Sov. J. Nucl. Phys. **15**, 438, 675 (1972); Y. L. Dokshitzer, Sov. Phys. JETP **46**, 641 (1977); G. Altarelli and G. Parisi, Nucl. Phys. **B126**, 298 (1977).

[56] J. Arrington *et al.*, Phys. Rev. C **64**, 014602 (2001).

[57] V. Tvaskis *et al.*, Phys. Rev. Lett. **98**, 142301 (2007).

[58] I. Niculescu, J. Arrington, R. Ent and C. E. Keppel, Phys. Rev. C **73**, 045206 (2006).

[59] M. Osipenko, W. Melnitchouk, S. Simula, S. A. Kulagin and G. Ricco, Nucl. Phys. **A766**, 142 (2006).

[60] W. Detmold, W. Melnitchouk and A. W. Thomas, Phys. Rev. D **66**, 054501 (2002).

[61] W. Detmold *et al.*, Phys. Rev. Lett. **87**, 172001 (2001).

[62] M. Osipenko *et al.*, Nucl. Phys. Proc. Suppl. **174**, 23 (2007).

[63] W. Melnitchouk, A. W. Schreiber and A. W. Thomas, Phys. Rev. D **49**, 1183 (1994); Phys. Lett. B **335**, 11 (1994).

[64] S. A. Kulagin, G. Piller and W. Weise, Phys. Rev. C **50**, 1154 (1994).

[65] S. A. Kulagin and R. Petti, Nucl. Phys. **A765**, 126 (2006).

[66] Y. Kahn, W. Melnitchouk and S. A. Kulagin, Phys. Rev. C **79**, 035205 (2009).

[67] W. Melnitchouk and A. W. Thomas, Phys. Lett. B **377**, 11 (1996).

[68] S. P. Malace, Y. Kahn, W. Melnitchouk and C. E. Keppel, Phys. Rev. Lett. **104**, 102001 (2010).

[69] A. Bodek *et al.*, Phys. Rev. D **20**, 1471 (1979); A. Bodek and J. L. Ritchie, Phys. Rev. D **23**, 1070 (1981).

[70] P. E. Bosted and M. E. Christy, Phys. Rev. C **77**, 065206 (2008).

[71] I. R. Afnan *et al.*, Phys. Lett. B **493**, 36 (2000); Phys. Rev. C **68**, 035201 (2003).

[72] E. Pace, G. Salme, S. Scopetta and A. Kievsky, Phys. Rev. C **64**, 055203 (2001).

[73] Jefferson Lab Experiment PR12-06-118, *Measurement of the F_2^n/F_2^p, d/u ratios and $A = 3$ EMC effect in DIS off the tritium and helium mirror nuclei*, G. G. Petratos contact person.

[74] L. L. Frankfurt and M. I. Strikman, Phys. Rept. **76**, 215 (1981); S. Simula, Phys. Lett. B **387**, 245 (1996); W. Melnitchouk, M. Sargsian and M. I. Strikman, Z. Phys. A **359**, 99 (1997).

[75] P. A. Souder, AIP Conf. Proc. **747**, 199 (2005).

[76] Jefferson Lab Experiment E12-10-107, *Precision Measurement of parity-violation in DIS over a broad kinematic range*, P. Souder contact person.

[77] T. Hobbs and W. Melnitchouk, Phys. Rev. D **77**, 114023 (2008).

[78] H. C. Fenker *et al.*, Nucl. Instrum. Meth. A **592**, 273 (2008).

[79] Jefferson Lab Experiment PR12-06-113, *The structure of the free neutron at large x-Bjorken*, S. Bültmann contact person.

[80] F. D. Aaron *et al.*, Phys. Lett. B **665**, 139 (2008).

[81] V. Tvaskis *et al.*, Phys. Rev. Lett. **98**, 142301 (2007).

[82] G. Altarelli, R. K. Ellis, G. Martinelli and S. Y. Pi, Nucl. Phys. **B160**, 301 (1979).

[83] A. Afanasev, C. E. Carlson and C. Wahlquist, Phys. Rev. D **62**, 074011 (2000).

[84] A. Accardi, T. Hobbs and W. Melnitchouk, JHEP **0911**, 084 (2009).

[85] E. L. Berger, Nucl. Phys. **B85**, 61 (1975); in Proceedings of the Workshop on Electronuclear Physics with Internal Targets, SLAC (1987).

[86] W. Melnitchouk, AIP Conf. Proc. **588**, 267 (2001).

[87] P. Geiger, Ph.D. dissertation, Heidelberg U. (1998); B. Hommez, Ph.D. dissertation, Gent U. (2003).

[88] J. Pumplin *et al.*, JHEP **0207**, 012 (2002); D. Stump *et al.*, JHEP **0310**, 046 (2003).

[89] Jefferson Lab Experiment E12-10-002, *Precision measurements of the F_2 structure function at large x in the resonance region and beyond*, S. P. Malace contact person.

[90] Jefferson Lab Experiment E12-06-104, *Measurement of the ratio $R = \sigma_L/\sigma_R$ in semi-inclusive DIS*, R. Ent contact person.